AIMETA '03
XVI Congresso AIMETA di Meccanica Teorica e Applicata
16th AIMETA Congress of Theoretical and Applied Mechanics

BIFURCATIONS AND SHEAR BANDS BY THE BOUNDARY ELEMENT METHOD

M. BRUN[1], D. BIGONI[1], D. CAPUANI[2]

[1] *Dipartimento di Ingegneria Meccanica e Strutturale, Università di Trento, Trento*
[2] *Dipartimento di Architettura, Università di Ferrara, Ferrara*

SOMMARIO
Per mezzo di una tecnica con elementi di contorno basata su una soluzione fondamentale proposta di recente, vengono analizzate deformazioni elastiche incrementali sovrapposte ad uno stato di deformazione omogenea. La formulazione, che racchiude in sè gli effetti delle grandi deformazioni, consente di determinare i carichi di biforcazione e gli associati modi di deformazione. In particolare, sono esaminati casi di biforcazione per strutture elastiche, comprendenti solidi fratturati e multilaminati, e, come casi speciali di instabilità senza una lunghezza caratteristica di scala, sono analizzate le biforcazioni di superficie e le *shear bands*.

ABSTRACT
Incremental elastic deformations superimposed upon a given homogeneous strain are analysed with a boundary element technique. This is based on a recently-developed Green's function for nonlinear incremental elastic deformations. Since the formulation fully embodies large strain effects, it allows for the determination of bifurcation loads and associated deformation modes. In particular, bifurcations of elastic structures are investigated, including cracked bodies and multilayers. As special cases of instability not involving length scales, surface bifurcations and shear bands are analysed.

1. INTRODUCTION

Surface instability and shear bands are two peculiar kinds of bifurcations, the latter corresponding to the condition of loss of ellipticity. Both bifurcations represent ill-posedness of the incremental problem and are characterised by the fact that the bifurcation mode embodies an arbitrarily short wave length. This gives rise to well-known difficulties in finite element simulations.

Many routes have been proposed to numerically regularise a problem *beyond* the elliptic range. In particular, a class of approaches consists in modifying the constitutive models to include an intrinsic characteristic length. Non-local constitutive models [7], Cosserat continua [3], visco-plastic models and higher-order gradient models [12] fall within this class. In

another class of approaches, numerical regularisation is pursued by introducing *ad hoc* special interpolating functions at the element level or by embedding strong discontinuities [2].

A common aspect of the above-mentioned strategies, is that they are aimed to restore the ellipticity of governing equations. In contrast to this general situation, the restoration of ellipticity is avoided in the approach of the present paper, since strain localisation is analysed in the *proximity* of the ellipticity boundary, as induced by a perturbation still inside the region of ellipticity. As a result of perturbation, introducing in a sense a length scale, localised deformation patterns emerge. The approach is based on a boundary element formulation where two-dimensional, incremental nonlinear deformations are considered from a given, homogeneously stressed configuration.

2. BOUNDARY INTEGRAL EQUATIONS

For an incompressible solid B, currently in a state of plane homogeneous finite deformation, the integral representations relating the velocity v_i and the pressure rate $\dot{p}$ in an interior point $\mathbf{y}$ of the body to the boundary values of velocities and nominal traction rates $\dot{\tau}_i$ are

$$v_g(\mathbf{y}) = \int_{\partial B} \left[\dot{\tau}_i(\mathbf{x}) v_i^g(\mathbf{x},\mathbf{y}) - \dot{\tau}_i^g(\mathbf{x},\mathbf{y}) v_i(\mathbf{x}) \right] dl_x \tag{1}$$

$$\begin{aligned} \dot{p}(\mathbf{y}) = & -\int_{\partial B} \dot{\tau}_g(\mathbf{x}) \dot{p}^g(\mathbf{x},\mathbf{y}) dl_x + \int_{\partial B} n_i(\mathbf{x}) v_j(\mathbf{x}) K_{ijkg} \dot{p}^g_{,k}(\mathbf{x},\mathbf{y}) dl_x \\ & - \left(4\mu\mu_* - 4\mu_*^2 + \mu\sigma - 2\mu_*\sigma - \frac{\sigma^2}{2} \right) \int_{\partial B} n_i(\mathbf{x}) v_i(\mathbf{x}) v^1_{1,11}(\mathbf{x},\mathbf{y}) dl_x \\ & - \sigma \left(\mu + \frac{\sigma}{2} \right) \int_{\partial B} n_i(\mathbf{x}) v_i(\mathbf{x}) v^2_{2,11}(\mathbf{x},\mathbf{y}) dl_x \end{aligned} \tag{2}$$

where n_i is the outward unit normal to the boundary ∂B, and v_i^g, $\dot{\tau}_i^g$, $\dot{p}^g$ are the velocity, the nominal traction rate and the pressure rate, respectively, of the Green fundamental state (see BIGONI & CAPUANI [1]). The tensor K_{ijkl} represents the instantaneous moduli which possess the major symmetry $K_{ijkl} = K_{klij}$ and are linear functions of the principal Cauchy stress components σ_1 and σ_2 ($\sigma = \sigma_1 - \sigma_2$ is the deviatoric in-plane stress) and of two incremental moduli μ and μ_* corresponding to shearing parallel to, and at 45° to, the principal stress axes.

If the point y is on the boundary, equation (1) becomes [1]

$$C_i^g v_i(\mathbf{y}) = \int_{\partial B} \dot{\tau}_i(\mathbf{x}) v_i^g(\mathbf{x},\mathbf{y}) dl_x - P.V. \int_{\partial B} \dot{\tau}_i^g(\mathbf{x},\mathbf{y}) v_i(\mathbf{x}) dl_x \tag{3}$$

where P.V. denotes the Cauchy principal value of the relevant integral and

$$C_i^g = \lim_{\varepsilon \to 0} \int_{\partial C_\varepsilon} \dot{\tau}_i^g(\mathbf{x},\mathbf{y}) dl_x \tag{4}$$

is the so-called **C**-matrix, depending on the material parameters, the state of pre-stress and the geometry of the boundary. In equation (4), the symbol ∂C_ε indicates the intersection between a circle of radius ε centred at **y** and the domain B.

Equation (3) is the basis of the collocation boundary element method. In the present paper, linear elements are adopted for the discretization of the boundary and integrals are computed numerically, using Gaussian quadrature formulae with 12 integration points for the Green functions and 18 points for the integrals in equation (3), unless otherwise specified.

3. BIFURCATION OF ELASTIC STRUCTURES

3.1. Elastic block

An elastic block is considered, in a square (the edge length has been taken equal to $2b$) stressed current configuration, for a Mooney-Rivlin material. A uniaxial state of stress is prescribed in terms of the non-dimensional parameter k defined as

$$k = \frac{\sigma}{2\mu} = \frac{\lambda_1^2 - \lambda_2^2}{\lambda_1^2 + \lambda_2^2} \tag{5}$$

where λ_1 and λ_2 are the in-plane stretches. Bifurcations from this state were analysed by HILL & HUTCHINSON (1975), considering a smooth bilateral constraint at the two edges normal to the direction of the uniaxial stress. For Mooney-Rivlin material, bifurcations are only possible in compression where it turns out that the first bifurcation occurs at $k \approx 0.522$, corresponding to an anti-symmetric mode with a ratio $\lambda/2b = 2$ between wave length and edge length. Above this bifurcation value, an infinite set of critical values of k follows, corresponding to anti-symmetric bifurcations. The accumulation point of these values defines the surface instability, occurring at $k \approx 0.839$, solution of the equation (see RADI *et al*. [8])

$$\frac{k}{2}\left(1 - \sqrt{\frac{1-k}{1+k}}\right) - 1 = 0 \tag{6}$$

and corresponding to the limit $\lambda/2b = 0$. For values of k greater than the surface instability threshold, an infinite set of symmetric bifurcation becomes possible, bounded by $k \approx 0.926$ for $\lambda/2b = 2/3$, which is the highest bifurcation value of k.

In order to analyse the problem by the boundary element method, two uniform meshes of 72 and 144 boundary elements (denoted as "coarse" and "fine" in the following) have been chosen. The upper and lower edges of the block have been constrained with smooth rigid boundaries, and the lower central node has been fixed to eliminate rigid body translation.

In the first example, the block is subjected to a horizontal anti-symmetric incremental dead-load $\dot{\tau}$ (Fig. 1). The loaded portion is equal to 1/9 of the total edge length. The velocity v_c at the upper corner is plotted versus the pre-stress k and comparison is made with results given by ABAQUS-Standard (Ver. 6-2-Hibbitt, Karlsson & Sorensen Inc.) with plane-strain 4-node bilinear hybrid elements (CPE4H). It can be seen that traction (i.e. negative values of k) increases stiffness, whereas compression induces stiffness degradation, which becomes dramatic when a critical value of k is reached corresponding to a Euler-type instability.

In the second example, the same block is subjected to a symmetric perturbation as is shown in Fig. 2. Here, it is evident that the finer is the mesh, the closest is the zero-stiffness asymptote to the surface instability ($k = 0.839$).

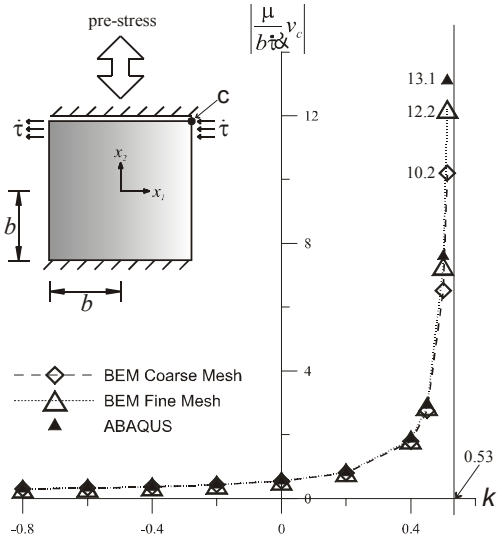

Fig. 1: Anti-symmetric perturbation

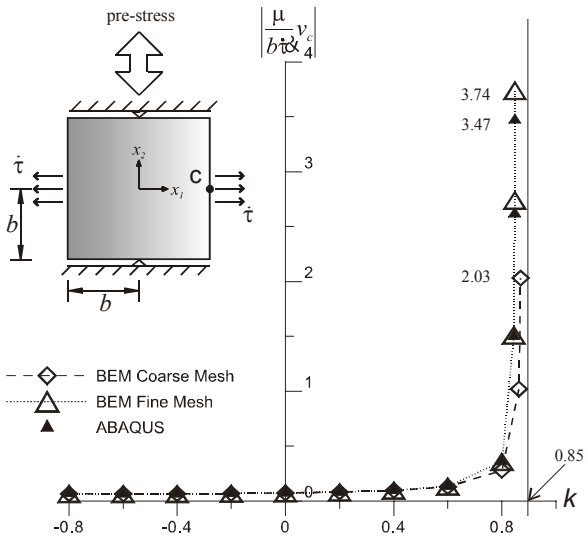

Fig. 2: Symmetric perturbation

Deformation modes associated with the anti-symmetric and the symmetric perturbation are shown in Figure 3 for different pre-stress levels.

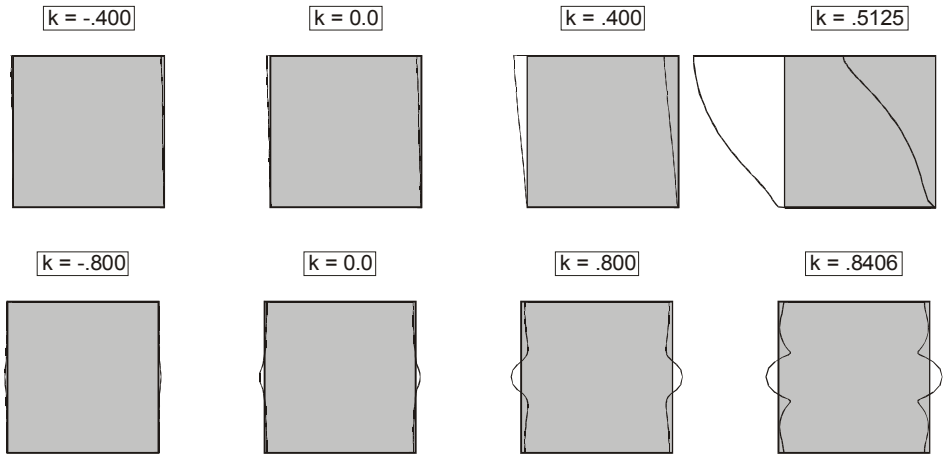

Fig. 3: Euler-type instability and surface instability

3.2. Layered elastic material

The layered elastic structure sketched in the detail of Fig. 4 is considered. The structure is made up of three layers, with a `material 1' common to the outer layers and a different `material 2' forming the core. Three cases are considered for the ratios of incremental shear moduli $[(\mu_*/\mu)_1, (\mu_*/\mu)_2, \mu_1/\mu_2]$ of the two materials ([1, 1/2, 1/2] in Case 1, [2/3, 1, 3/2] in Case 2, [1/2, 1, 2] in Case 3). All layers are specified to undergo the same homogeneous, plane strain deformation with the principal directions of deformation aligned normal and parallel to the layers. Therefore, a uniaxial state of traction or compression prevails in the laminate. Starting from this pre-stressed state, an incremental, horizontal anti-symmetric loading $\dot{\tau}$ is prescribed applied on a loading zone equal to $2b/15$. The results, with a uniform

mesh of 80 elements for each layer, are reported in Fig. 4 where the velocity is plotted versus the pre-stress k. It should be noted that the values of k are independent of the material, since they depend only on the in-plane stretch (5), identical in all layers.

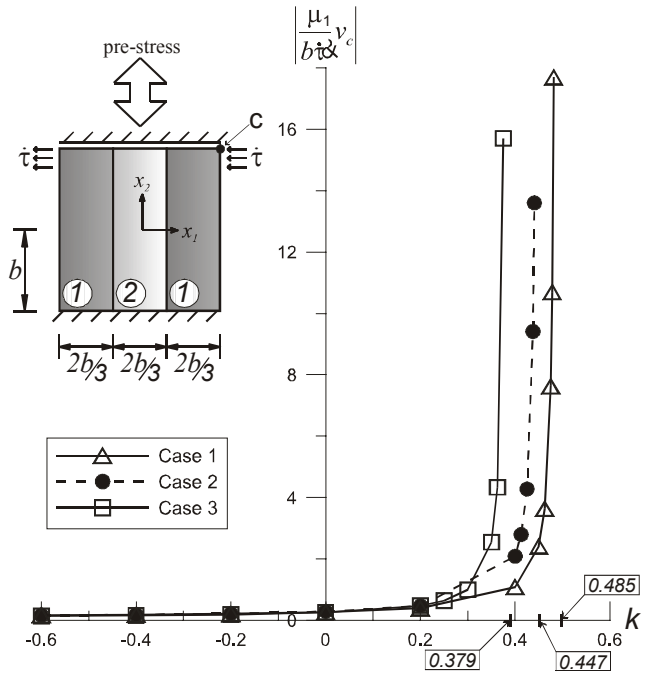

Fig. 4: Anti-symmetric bifurcation of a laminate

3.3. Cracked elastic blocks

A pre-stressed, rectangular (3b×2b) elastic block is considered, containing cracks parallel to the free edges. Three cracked configurations are chosen as sketched in the particular of Fig. 5 and the response to a symmetric perturbation is analysed at different levels of pre-stress k.

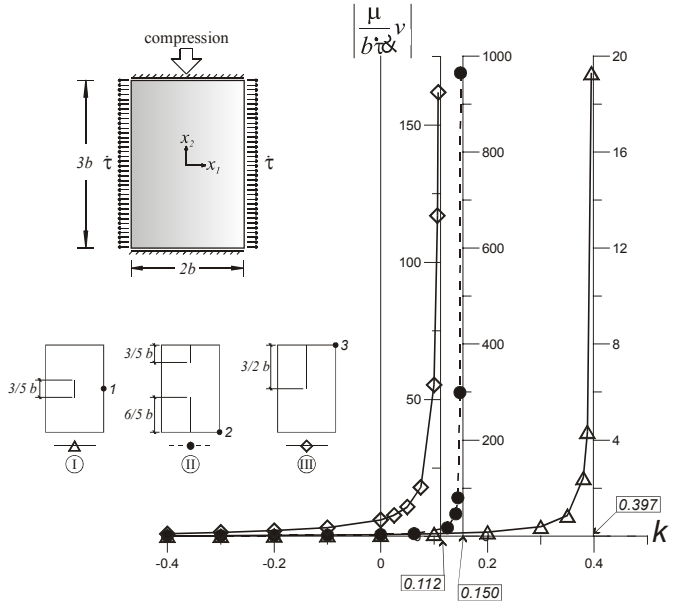

Fig. 5: Bifurcation for three different cracked configurations

The perturbation consists of a uniform nominal loading rate along the entire lateral edges which are free until the instant of the perturbation, inducing Mode I near-tip fields. For this situation, no analytical solutions are available, with the exception of the asymptotic near-tip representation obtained by RADI *et al*. [8]. The incremental displacements at a characteristic point of each cracked geometry are plotted in Fig. 5 where the asymptotes correspond to the first bifurcation value k = 0.112, 0.150, 0.397. The deformed configurations of the cracked bodies, for values of *k* close to bifurcation are illustrated in Fig. 6. In the analysis the unilateral contact of the crack faces has been taken into account. A peculiar effect is visible in the geometry II of Fig. 6, where the upper crack remains closed, due to the high value of *k*. Analyses not reported here have shown that the same crack opens for values of k = 0.0625.

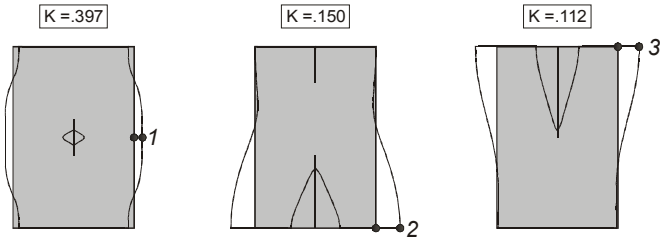

Fig. 6: Incremental displacements in proximity of bifurcation

4. SHEAR BANDS WITHIN THE ELLIPTIC RANGE

For the incompressible body under consideration, the constitutive equation relating the material derivative of nominal stress to the velocity gradient can be written as

$$\dot{t}_{ij} = K_{ijkl} v_{l,k} + \dot{p}\delta_{ij}, \qquad v_{i,i} = 0, \tag{7}$$

It is well-known that shear bands represent an extreme form of material instability, corresponding to failure of ellipticity

$$n_i K_{ijhk} n_h g_k = 0, \quad \text{subject to} \quad n_k g_k = 0, \tag{8}$$

for at least one unit vector n_k and non-null orthogonal vector g_k.

In a continuous loading program, loss of ellipticity can occur after various bifurcation thresholds are attained. For instance, in the examples presented in the previous Section shear bands may only occur well after the detected bifurcation points. As a consequence, shear banding must be analysed when the structure is in a post-critical range (a circumstance usually overlooked in the literature). This is not an easy task, since in that case the current state is inhomogeneous. However, there is a special case where shear bands may occur as the first possible bifurcation. This is the so-called "van Hove condition", in which the solid is subject to prescribed displacements over the entire boundary and the current state (deformation and stress) is homogeneous (VAN HOVE, 1947). More in detail, the incremental solution is unique - unless an arbitrary uniform pressure - until the strong ellipticity condition holds

$$n_i K_{ijhk} n_h g_k > 0, \quad \text{subject to} \quad n_k g_k = 0, \tag{9}$$

for all pair of orthogonal vectors n_k and g_k. However, it is clear that the first failure of strong ellipticity in a continuous loading program corresponds to failure of ellipticity and shear band formation. Therefore, we consider van Hove conditions, assuming the geometric setting shown in Fig. 7, where a square elastic block is considered, homogeneously deformed in a state of uniaxial tension or compression. Displacements are prescribed on the entire boundary, so that the solution is known unless an arbitrary value of homogeneous pressure. We assume $\mu_*/\mu=0.25$, corresponding to the elliptic complex regime, and perturb this configuration prescribing the triangular distributions of velocity sketched in Fig. 7.

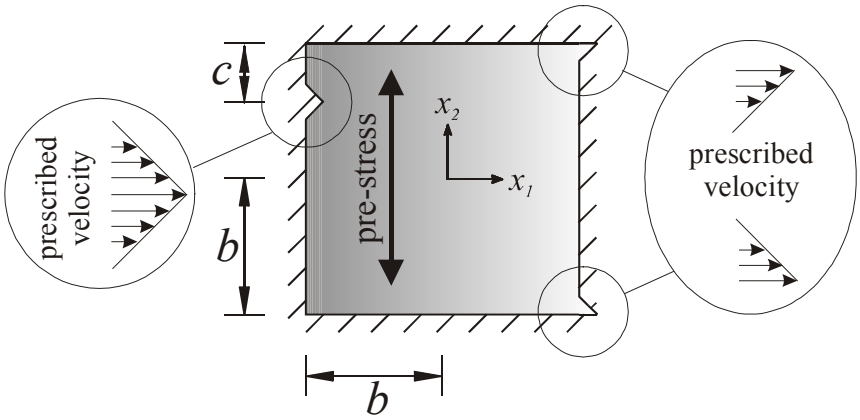

Fig. 7: Van Hove condition

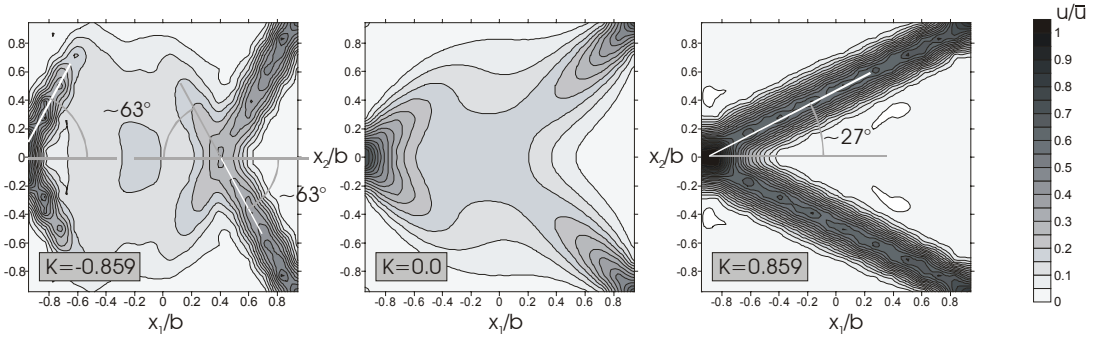

Fig. 8: Level sets of velocity in the van Hove condition

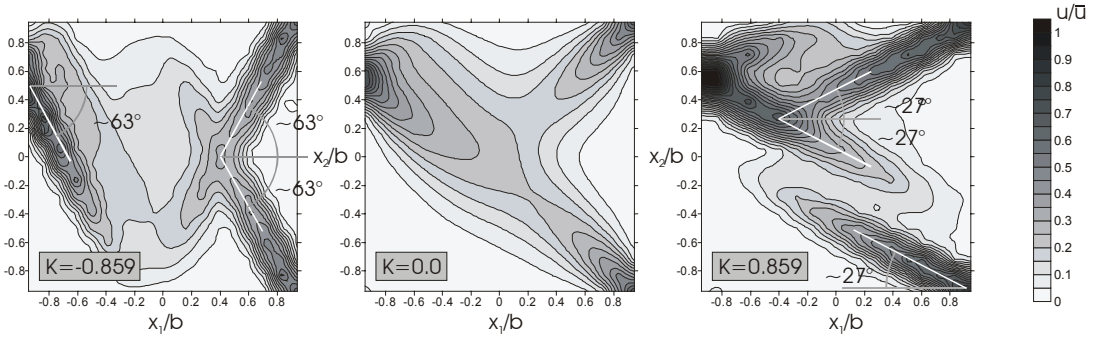

Fig. 9: Level sets of velocity in the van Hove condition

The perturbation is characterised by the ratio of the maximum assigned velocity to the length of the application zone. This ratio has been assumed equal to 9/20 and 9/40 on the left

and right edge, respectively, of the block in Fig. 7. Results of computations - in terms of level sets of the velocity modulus - are reported in Fig. 8 and 9, the former relative to c/b=1/2, the latter to c/b=4/9.

A 144-element uniform mesh has been employed to discretize the boundary and a 324-point uniform grid has been used to evaluate the interior velocity field. The Gauss points for the numerical integrations have been increased to 48. Three different situations are reported in the figures, corresponding to three different values of pre-stress k = -0.859, 0, 0.859. The values ±0.859 are close to the boundary of loss of ellipticity, occurring at $k = \pm 0.866025$.

When the elliptic boundary is attained, shear bands become possible, inclined at an angle η solution of the equation (HILL AND HUTCHINSON, 1975)

$$\tan^2 \eta = \frac{1 + 2\sqrt{\mu_* / \mu (1 - \mu_* / \mu)}}{1 - 2\,\mu_* / \mu}, \tag{10}$$

which, in the special case of $\mu_*/\mu = 0.25$, gives a band inclination $\eta = 27.367°$, with respect to the direction of the maximum in-plane stress component.

It can be seen from Fig.8 and Fig. 9 that when the elliptic boundary is approached, the velocity tends to localise along well-defined shear band patterns. They highlight the inclinations of the discontinuity bands formally possible only at the elliptic boundary. The fact that strain localisation can be observed within the elliptic range employing a perturbation approach agrees with findings by BIGONI & CAPUANI [1]. On the other hand, it may provide an explanation of the fact that shear banding is a preferred instability when compared to other diffuse bifurcations, possible at loss of ellipticity under van Hove conditions (RYZHAK, 1999).

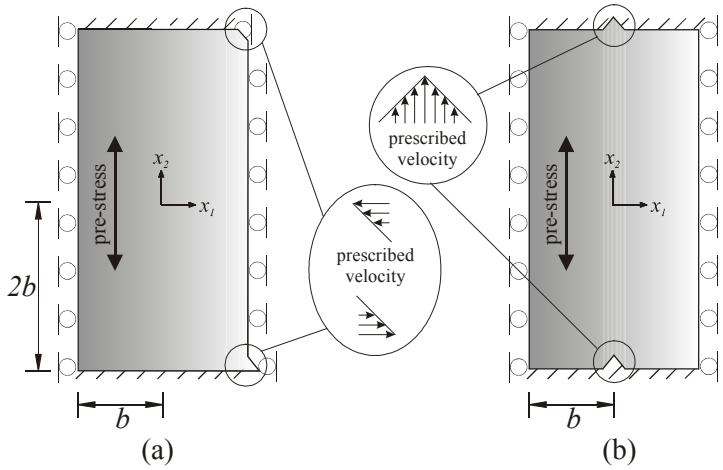

Fig. 10: Weak van Hove condition

The van Hove conditions are very peculiar and provide the maximum possible confinement to a material sample. Referred to the case of compressible materials, RYZHAK (1993, 1994) has shown that the van Hove theorem can be extended to a less restrictive condition, that will be called `weak van Hove' in the following. In particular, the material must be homogeneous and orthotropic, with orthotropy axes parallel and orthogonal to the given loading direction. Instead of the usual prescription on displacement, now two parallel edges can be in smooth (bilateral) contact with a rigid constraint (the lubricated ends employed by Biot to explain the so-called "internal instabilities"). This is the situation

sketched in Fig. 10 which we employ as a current configuration to be perturbed with two assigned, triangular velocity distributions.

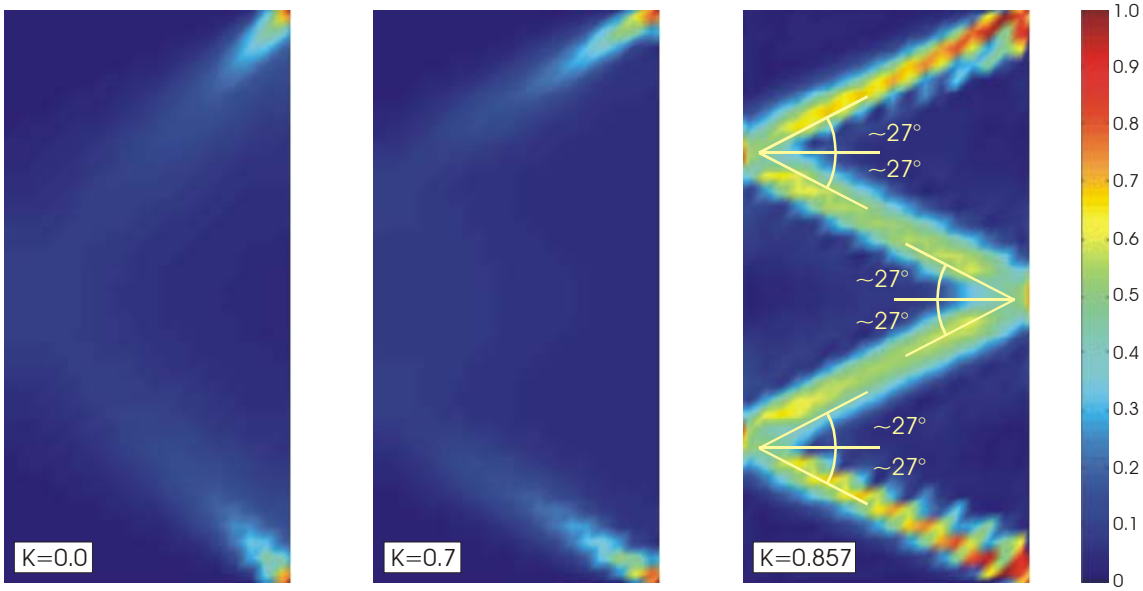

Fig. 11: Level sets of velocity in the weak van Hove condition

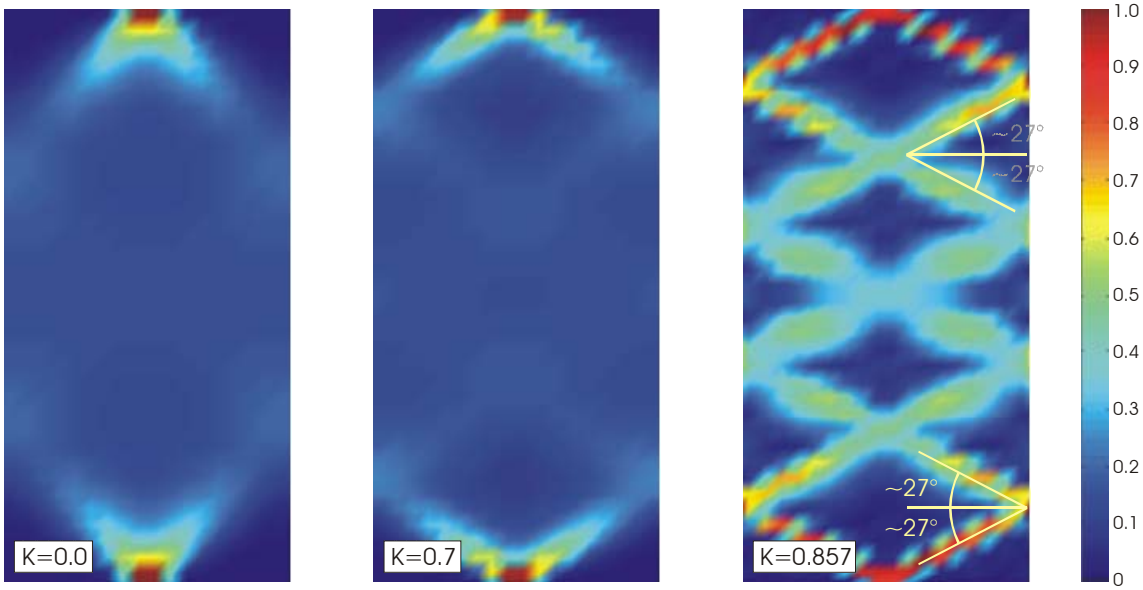

Fig. 12: Level sets of velocity in the weak van Hove condition

As in van Hove conditions, the current situation is again defined unless an arbitrary value of homogeneous pressure. Level sets of the velocity are plotted in Figs. 11 and 12 for different values of pre-stress k = 0, 0.7, 0.857 corresponding to compression parallel to x_2. A 216-elements, uniform mesh has been employed for the boundary and 648 points for the evaluation at the internal points. Again, the Gauss points have been increased to 48 for the evaluation of integrals. We may note that until k = 0.7 there is no much evidence of shear banding, but this becomes evident when the boundary of loss of ellipticity is approached with k = 0.857.

The examples of Figs. 11-12 show that peculiar deformation patterns emerge, due to "reflection" of shear bands at the boundary. This feature of localised deformation has been observed in different contexts (behaviour of porous plastic materials, TVERGAARD [13]) and could be exploited to explain pattern formation in living tissues or in geological structures. In particular, the adaptative substructuring of trabecular bone shown by HUISKES *et al*. (2000, their Fig. 4) displays similarities to the pattern of Fig. 11 whereas the deformation patterns in granular media evidenced by DESRUES & CHAMBON (2002, their Fig. 4) exhibit a similarity to the pattern of Fig. 12. The obtained patterns of deformation may also suggest a number of technological applications. For instance, we may easily speculate that the highly strained regions could transmit signals in a very localised way, so that the pre-stress may become a parameter controlling delay lines with special properties.

REFERENCES

[1] Bigoni D., Capuani D.: Green's function for incremental nonlinear elasticity: shear bands and boundary integral formulation, *J. Mech. Phys. Solids* Vol. 50, pp. 471-500 (2002).

[2] Boria R.I.: Finite element simulation of strain localization with large deformation: capturing strong discontinuity using a Petrov-Galerkin multiscale formulation, *Comp. Meth. Appl. Mech. Engng.*, Vol. 191, pp. 2949-2978 (2002).

[3] de Borst, R., Sluys, L.J.: Localization in a Cosserat continuum under static and dynamic loading conditions, *Comp. Meth. Appl. Mech. Engrg.,* Vol.90, pp. 805-827 (1991).

[4] Desrues J., Chambon R.: Shear band analysis and shear moduli calibration, *Int. J. Solids Structures* Vol. 39, pp. 3757-3776 (1999).

[5] Hill R., Hutchinson J.W.: Bifurcation phenomena in the plane tension test, *J. Mech. Phys. Solids* Vol. 23, pp. 239-264 (1975).

[6] Huiskes R., Ruimerman R., van Lenthe G.H., Janssen J.D.: Effects of mechanical forces on maintenance and adaptation of form in trabecular bone, *Nature* Vol. 405, pp. 704-706 (2000).

[7] Leblond, J.B., Perrin, G., Devaux, J.: Bifurcation effects in ductile metals with nonlocal damage, *J. Appl. Mech.* Vol. 61, pp. 236-242 (1994).

[8] Radi E., Bigoni D., Capuani D.: Effects of pre-stress on crack-tip fields in elastic, incompressible solids, *Int. J. Solids Structures* Vol. 39, pp. 3971-3996 (2002).

[9] Ryzhak E.I.: On stable deformation of "unstable" materials in a rigid triaxial testing machine, *J. Mech. Phys. Solids* Vol. 41, pp. 1345-1356 (1993).

[10] Ryzhak E.I.: On stability of homogeneous elastic bodies under boundary-conditions weaker than displacement conditions, *Quart. J. Mech. Appl. Math.* Vol. 47, pp. 663-672 (1994).

[11] Ryzhak E.I.: A case of indispensable localized instability in elastic-plastic solids, *Int. J. Solids Structures* Vol. 36, pp. 4669-4691 (1999).

[12] Sluys, L.J., Estrin, Y.: The analysis of shear banding with a dislocation based gradient plasticity model, *Int. J. Solids Structures* Vol. 37, pp. 7127-7142 (2000).

[13] Tvergaard V.: Influence of void nucleation on ductile shear fracture at a free surface, *J. Mech. Phys. Solids* Vol. 30, pp. 399-425 (1982).

[14] van Hove L.: Sur l'extension de la condition de Legendre du calcul des variations aux intégrales multiples à plusieurs fonctions inconnues, *Proc. Sect. Sci. K. Akad. van Wetenschappen*, Amsterdam, Vol. 50, pp. 18-23 (1947).